



CHORUS

This is the accepted manuscript made available via CHORUS. The article has been published as:

Testing the limits of the spatial Markov model for upscaling transport: The role of nonmonotonic effective velocity autocorrelations

Nicole L. Sund, Diogo Bolster, and David A. Benson

Phys. Rev. E **94**, 043107 — Published 13 October 2016

DOI: [10.1103/PhysRevE.94.043107](https://doi.org/10.1103/PhysRevE.94.043107)

Testing the limits of the Spatial Markov model for upscaling transport: the role of non-monotonic effective velocity autocorrelations

Nicole L Sund^{1,2*} and Diogo Bolster², David A Benson³

¹*Division of Hydrologic Sciences, Desert Research Institute, Reno, NV 89512, USA*

²*Dept. of Civil and Environmental Engineering and Earth Sciences,*

University of Notre Dame, Notre Dame, IN 46545, USA

³*Dept. of Geology and Geological Engineering,*

Colorado School of Mines, Golden, CO 80401, USA

Abstract

The Spatial Markov model is a Lagrangian random walk model, widely and successfully used for upscaling transport in heterogeneous flows across a broad range of problems. It is particularly useful at early or pre-asymptotic times when many other conventional upscaling approaches may not be valid. However, as with all upscaled models, it must have its limits. In particular, the question of what the smallest scale at which it can be legitimately applied, without violating implicit assumptions, remains. Here we address this issue by considering one of the most classical transport upscaling problems: Taylor dispersion in a bounded shear flow. We demonstrate that the smallest scale for the Spatial Markov model depends on the transverse width of the domain, the variability of the flow field as quantified by a coefficient of variation, and the competition of longitudinal and transverse diffusion coefficients. We show that this scale is a factor of the Peclet number smaller than the classical Taylor dispersion scale, meaning that for advection-dominated systems where Peclet numbers are large, this model can be applied at much smaller scales than classical Taylor-Aris dispersion theories.

PACS numbers:

*E-mail: nsund@dri.edu

I. INTRODUCTION

Upscaling of transport in heterogeneous velocity fields is a long-standing discipline that aims to describe transport at some scale with a model that does not explicitly resolve all of the small-scale features of the flow that influence transport, but rather captures their influence in an effective manner. One of the most seminal examples is the early work of Taylor and Aris [1, 2], who showed that given sufficient time, transport of a solute flowing through a circular tube can be adequately described by a one-dimensional advection-dispersion equation with an effective dispersion coefficient that depends on the structure of the velocity field and magnitude of the molecular diffusion coefficient. Their ideas hold for any shear flow in a bounded domain. Other approaches, including the method of moments [3], volume averaging [4], and homogenization [5] generalize these ideas to more complex flow configurations. While these ideas are significant, it is important to recognize that in all these approaches, the use of a constant effective dispersion coefficient is only valid at asymptotic times. This asymptotic Taylor timescale is set by the amount of time it takes for a solute to sample the full range of velocities in the flow by diffusion; i.e. these approaches are valid for $t > \tau_D = L^2/D$, where L is a characteristic length scale of the system and D is the diffusion coefficient.

Prior to this asymptotic time, transport often displays anomalous behavior (i.e., a scaling of the second centered moment of a plume which is nonlinear in time). Depending on the application of interest, one may wish to make predictions of transport at times before this asymptotic time scale and consequently many of the aforementioned approaches have been further generalized to capture pre-asymptotic effects and effectively describe transport at times before the asymptotic Taylor timescale [6].

One model that has emerged recently and appears capable of capturing anomalous and pre-asymptotic transport in non-uniform flows is the Spatial Markov model, which was originally proposed by [7] to upscale transport in flows through highly heterogeneous porous media, building on a rich history of anomalous transport models [8–12]. The model falls into the category of random walk models, where a plume is discretized into a large number of particles which transition through space and time, following probabilistic rules that aim to reproduce the influence of small scale flow heterogeneity. In all of the applications of the Spatial Markov model to date [7, 13–21] the spatial jumps that particles make are fixed in

size and the time steps between jumps are random. What distinguishes this model from previous ones is that the successive temporal jumps are not independent, but rather are correlated. This enables the model to predict earlier pre-asymptotic transport behaviors than other approaches, which neglect such correlations.

As already noted, the model in its first application was used to upscale transport in a variety of highly heterogeneous permeability fields, including multigaussian, connected and stratified fields [7, 13]. Since then it has been successfully applied to a variety of other setups, including fractured media [14], synthetic [15, 16] and realistic [17] pore scale systems, steady and unsteady flows through porous media where inertial effects dominate [18, 19], reactive transport [20], and recently its first application to field-scale data, from a fractured aquifer [21]. While these successes demonstrate the great potential for this model, as with any upscaled model, it must have restrictions on its applicability; in particular, there must be a minimum scale in time and/or space above which it can be reliably used, but below which it does not hold. As noted above, classical Taylor dispersion models are only valid for times greater than the characteristic diffusion time. While we have abundant evidence that the Spatial Markov model is not as restricted, here we ask what its restrictions are; that is, at what spatiotemporal scales is it valid to use the Spatial Markov upscaling approach? This is the primary focus of this note.

To address this issue we return to a problem similar to Taylor's original one, which has received and continues to receive [22, 23] a great deal of attention. We focus on upscaling transport in shear flows in bounded domains, the asymptotic behavior of which is established and well understood. In particular, we aim to demonstrate limitations of the Spatial Markov model and define scales after which it may be reliably applied. We focus on these simple cases, because it makes the problem more tractable and elucidates certain critical points that are missed in more complex flows. Specifically we ask, how does one choose the size of the fixed spatial jump that particles take in the random walk sequence? More specifically, how small can it be, thus setting a scale below which the model may not hold.

II. SYSTEMS UNDER CONSIDERATION

A. Flow

The work considered here is restricted to purely shear flows that are physically bounded. Specifically, we consider solute transport in steady flow between two parallel plates positioned respectively at $y = 0$ and $y = L$ with average velocity \bar{u} between these two plates. To begin, we consider two steady classical flows, that is, linear Couette (u_c) and parabolic Poiseuille flow (u_p) [24], defined by

$$u_c(y) = \frac{2\bar{u}}{L}y \quad (1)$$

and

$$u_p(y) = \frac{6\bar{u}}{L^2}y(L - y). \quad (2)$$

Both these setups only have flow in the longitudinal (x) direction and the velocity is zero in the transverse (y) direction.

B. Transport

We consider transport of a conservative solute in these systems. The concentration of the solute (C) is governed by the advection diffusion equation,

$$\frac{\partial C}{\partial t} + u(y)\frac{\partial C}{\partial x} = D_L\frac{\partial^2 C}{\partial x^2} + D_T\frac{\partial^2 C}{\partial y^2}, \quad (3)$$

where $u(y)$ is the velocity in the longitudinal direction defined above and D_L and D_T are constant diffusion coefficients in the longitudinal and transverse directions, respectively. While diffusion is generally considered to be isotropic ($D_L = D_T$), it is convenient to distinguish between the two in the derivations below, because it turns out that they can compete with one another. Furthermore, while in classical flows like this it is unlikely that they will differ, in systems where one level of upscaling has already occurred D_L and D_T may represent anisotropic dispersion coefficients [25]. Throughout this study we will always consider an infinite domain in the longitudinal direction and a unit mass pulse initial condition. Boundary conditions at the vertical boundaries are no-flux.

We model Eq. 3 at this small scale using an equivalent random walk model [26]. The mass of the solute is split into a large number of discrete particles of equal mass whose motion is governed by the Langevin equation,

$$\begin{aligned} x_{n+1} &= x_n + u(y_n)\Delta t + \sqrt{2D_L\Delta t}\xi_n \\ y_{n+1} &= y_n + \sqrt{2D_T\Delta t}\eta_n \quad n = 0, 1, 2, \dots \end{aligned} \quad (4)$$

where $\{\xi_n\}$ and $\{\eta_n\}$ are independent samples from a standard Gaussian distribution (with mean zero and unit variance) and Δt is a fixed time step. The initial condition is imposed by placing all particles initially at $x = 0$ and distributing them across $0 < y < L$ such that the number of particles at each y location is proportional to the velocity at that location. The no flux conditions on the vertical boundaries are imposed by reflecting particles elastically off the boundaries.

C. Transport Behavior

1. Second Centered Spatial Moment

One of the most common metrics used to study transport behavior and to test the success of an upscaled model against is the temporal evolution of the second centered spatial moment in the longitudinal direction of the solute plume, $\sigma^2(t)$. This is a measure of longitudinal spreading, and is defined by,

$$\sigma^2(t) = \int_{-\infty}^{\infty} x^2 C dx - \left(\int_{-\infty}^{\infty} x C dx \right)^2, \quad (5)$$

or in terms of discrete particles used in the random walk simulations

$$\sigma^2(t) = \frac{1}{N} \sum_{i=1}^N x_i^2 - \left(\frac{1}{N} \sum_{i=1}^N x_i \right)^2. \quad (6)$$

An example of the evolution of the second centered moment over time is shown in Fig. 1 (a) for Couette flow with $L = \bar{u} = 1$ and $D_L = D_T = 10^{-3}$. Changing these parameters changes where transitions in these curves happen, but not general shape or trends. At very small times, the second centered moment scales linearly in time; then, at intermediate times it scales faster than linearly in time; and finally, at late times it returns to scaling linearly in time again. This behavior is well known and understood [27–29]. At the smallest times,

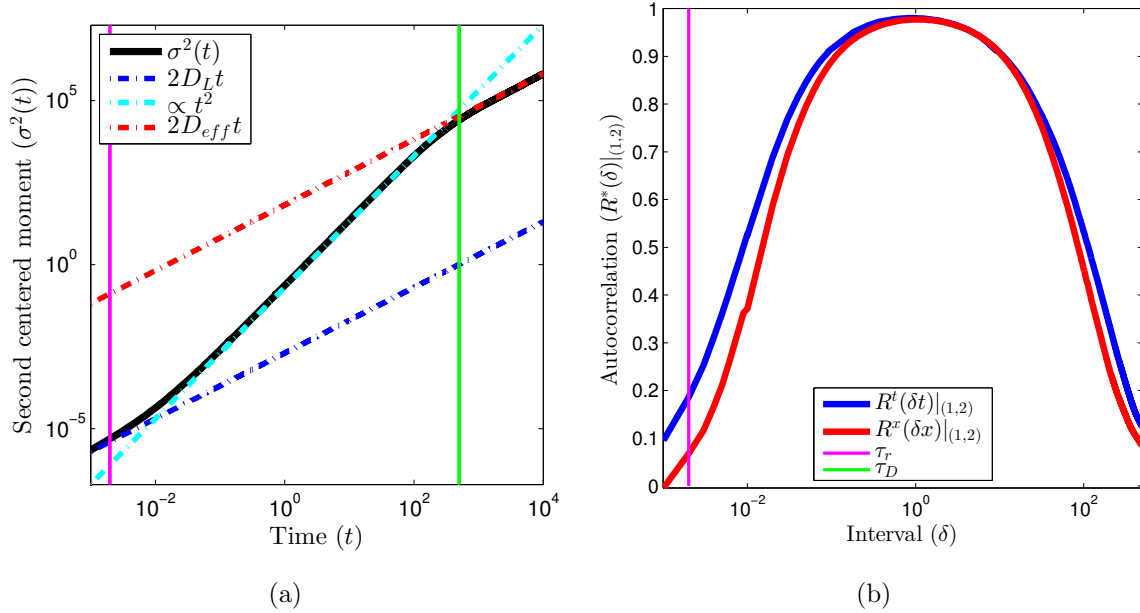


Figure 1: (a) Second centered spatial moment and (b) autocorrelation between velocities over the first set of successive time intervals of length δt and space intervals of length δx in Couette flow with $L = \bar{u} = 1$, and $D_L = D_T = 10^{-3}$, which demonstrate the transport behavior of the solute within each of the three transport regimes. The vertical lines mark the time scales where the system starts to behave ballistically (magenta line) and when the system returns to behaving diffusively again (green line).

longitudinal diffusion dominates the scaling; at intermediate time the non-uniform nature of the flow leads to rapid spreading with particles on fast streamlines persisting on fast streamlines and particles on slow streamlines remaining on slow streamlines; finally after the Taylor dispersion time when transverse diffusion has enabled all particles to sample all velocities, the system returns to behaving diffusively, but with a new larger effective dispersion coefficient, quantified by the Taylor dispersion coefficient. Thus there are two critical time scales in this process, that is when the system starts to behave ballistically and when the system returns to behaving diffusively again. These times are qualitatively illustrated by the vertical lines in Fig. 1.

2. Velocity Autocorrelations

Here we define another metric, much less commonly used but useful in characterizing the limitations of the Spatial Markov model, that is the autocorrelation of a particle's average effective velocity over a fixed increment in time or space [13, 16, 30]. Full details of the Spatial Markov model are provided in section IV. Briefly, it is a model that falls into the broader category of continuous time random walk models (CTRW). As such, understanding the spatial and temporal increments of a particle's motion is key to its successful implementation. This can be considered from the perspective of effective velocities. For each particle we track with (4), we can define an average effective velocity over a sequence of fixed increments in time (δt) and/or in space (δx) as,

$$v_i^t(\delta t) = \frac{\lambda_i}{\delta t}, \quad v_i^x(\delta x) = \frac{\delta x}{\tau_i}, \quad (7)$$

where λ_i is the distance a particle travels during the i^{th} time step, which is of size δt . Likewise τ_i is the amount of time it takes the particle to traverse the i^{th} space step of length δx . In this definition δt and δx are fixed, while λ and τ are measured from the small scale simulations. The superscripts in Eq. 7 define which dimension the effective velocities depend on. It is critical to note that both diffusion and advection in the small scale flow contribute to the specific values of $v_i^t(\delta t)$ and $v_i^x(\delta x)$, which are not physical velocities, but effective ones that lump these processes together.

In order to more clearly explain and interpret these effective velocities, a sample particle trajectory is shown in Fig. 2. At the very top of the figure, the path of a particle (starting at $x = 0, y = 0.5$) is shown. This path was generated using the Langevin equation (Eq. 4) with a small time step $\Delta t = 10^{-3}$ and can be considered a full representation of the path the particle follows. On the next level we do not resolve the full path of the particle, but rather look at it from an upscaled perspective and portray snapshots of it at given points in space and time. On the right hand side we fix the spatial increment δx (in this example $\delta x = 10$) as can be seen by the equidistant vertical black lines. The amount of time it has taken the particle to get between these points is not constant, which can be seen more clearly on the lowest tier of the figure where the longitudinal position of the particle against its point in time is shown. On the left hand side we look at the exact same trajectory, but this time consider a fixed temporal increment δt (in this example $\delta t = 10$). Now the vertical lines are

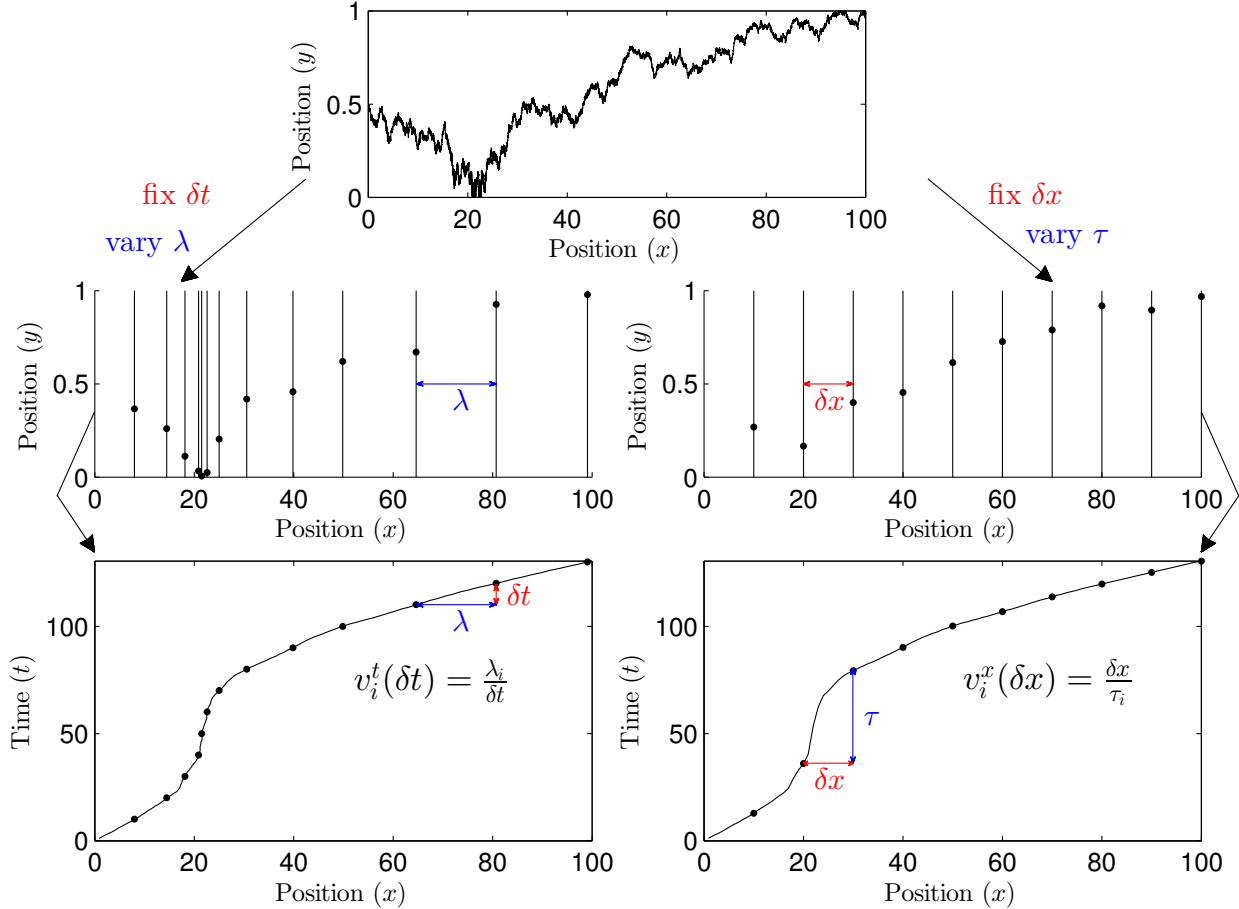


Figure 2: A sample particle trajectory in a Couette flow starting at $(x = 0, y = 0.5)$. On the left hand side we demonstrate how this path can be interpreted in an upscaled manner by looking at the evolution of the longitudinal position of the particle over fixed snapshots in time (fixed δt). On the right hand side we interpret the same path, but rather than taking observations at fixed snapshots in time we take the snapshots at fixed locations in longitudinal direction (fixed δx). On the bottom row we demonstrate how these different interpretations define the respective effective velocities in Eq. 7.

not equidistant in x , but the amount of time it has taken to get between them is fixed. The transitions that occur when the particle is close to the lower boundary are small for a fixed δt , which is completely in line with the fact that the velocity there is smaller. Similarly, these locations have been plotted on an x, t plot at the bottom. These figures demonstrate how we define the effective average velocities defined in Eq. 7.

Accepting these definitions we can now define autocorrelation functions for these velocities averaged over intervals of length δ as

$$R^*(i, j, \delta) = \frac{\text{Cov}[v_i^*(\delta), v_j^*(\delta)]}{\sqrt{\text{Cov}[v_i^*(\delta), v_i^*(\delta)] \text{Cov}[v_j^*(\delta), v_j^*(\delta)]}} \quad (8)$$

where $\text{Cov}[v_i^*(\delta), v_j^*(\delta)]$ is the covariance of $v_i^*(\delta)$ and $v_j^*(\delta)$, which are defined for $\delta = \delta x$, and $\delta = \delta t$ above. $R^*(i, j, \delta)$ is a function of i, j , and δ . Recall i and j are the indices of the steps taken of length δ . We will use the convention $R^*(i, j)|_\delta$ to refer to the autocorrelation between $v_i^*(\delta)$ and $v_j^*(\delta)$ for a fixed δ , and we will use the convention $R^*(\delta)|_{(i,j)}$ to refer to the autocorrelation between $v_i^*(\delta)$ and $v_j^*(\delta)$ for fixed i and j . Of particular interest here is $R^*(\delta x)|_{(1,2)}$, which is the autocorrelation between the first two effective velocities averaged over varying δx , because these are the effective velocities used to create the Spatial Markov model.

An example of these metrics is shown in Fig. 1 (b) for the same Couette flow configuration as noted above (i.e. $L = \bar{u} = 1$ and $D_L = D_T = 10^{-3}$). Again, different choices of parameters may change the magnitude and transition locations of these curves, but not the overall shape, which we focus on here. The autocorrelation function shown in Fig. 1 (b) is for velocities measured over the first two consecutive intervals of varying length δ , where we use δ to generically refer to either δx or δt , so that $i = 1, j = 2$ in Eq. 8 above. Over very early times/small spatial increments, correlation effects are weak. Over this scale, transport is dominated by longitudinal diffusion (still in the pre-asymptotic Fickian scaling regime for the second centered moment which is shown in Fig. 1 (a)). The autocorrelation function ($R^*(\delta)|_{(1,2)}$) is near zero here, because diffusion is inherently an uncorrelated process. Over intermediate δ , when $\sigma^2(t)$ grows faster than linearly in time (in this case it is ballistic, $\sigma^2(t) \sim t^2$), advection has overcome diffusion and $R^*(\delta)|_{(1,2)}$ begins to increase - advection induces correlation [31]. In the absence of diffusion a given particle would always stay on the same streamline so its effective velocities would be the actual advective velocity, which would never change and so be perfectly correlated. Throughout this regime, $R^*(\delta)|_{(1,2)}$ increases to a peak. After the peak, the autocorrelation function decreases again (note that the shape of the curves appears to be close to symmetric in log space). Finally, over large δ , when the second centered moment transitions back to a linear regime ($\sigma^2(t) = 2D_{\text{eff}}t$, where D_{eff} is a constant dispersion coefficient), $R^*(\delta)|_{(1,2)}$ drops back down to near zero, which reflects the fact that pure Fickian dispersion is an uncorrelated process. This is the asymptotic, or Taylor, regime, where the solute has had sufficient time to sample the entire velocity field

and the motions in the longitudinal direction can be fully described by a one dimensional Fickian advection-dispersion equation.

III. THE PEAK IN THE AUTOCORRELATION FUNCTION

As an initial estimate we postulated that the location of the peak in the autocorrelation functions defined in Eq. 8 and depicted graphically in Fig. 1 would set the smallest scale over which the Spatial Markov could be applied. As will become clearer further on, the peak is not sufficient and underestimates the true scale. Nonetheless it will be useful to consider.

A. Scaling Arguments for the Peak Location of the Autocorrelation Function

In order to find the location of the peaks of the autocorrelation functions, we must first define the time scales that separate the three transport regimes discussed in II C. These are the time scales where the autocorrelation function transitions from being near zero to non-negligible and transitions back again. Transport in the longitudinal direction causes the increase in the autocorrelation function and transport in the transverse direction causes the fall in the autocorrelation function. This is clear by closely examining the Langevin equation (Eq. 4).

In the longitudinal direction, transport is due to both advection and diffusion,

$$x^{n+1} = x^n + \underbrace{u\Delta t}_{\text{advective length}} + \underbrace{\sqrt{2D_L\Delta t}\xi_n}_{\text{diffusive length}} \quad n = 0, 1, 2, \dots \quad (9)$$

For very small Δt , the diffusive length tends to be larger than the advective length (because $\sqrt{\Delta t} \gg \Delta t$). This leads to an essentially uncorrelated process because the random noise (diffusion) dominates the deterministic step (advection). If we set the typical advective step to be $\bar{u}\Delta t$ and the typical noise due to the diffusive step to be $\sqrt{2D_L\Delta t}$, then we can expect that the onset of the rise of the autocorrelation function will occur at the time when these step sizes become equal. Let us denote this as the rising time τ_r ,

$$\begin{aligned} \bar{u}\tau_r &= \sqrt{2D_L\tau_r} \\ \implies \tau_r &= \frac{2D_L}{\bar{u}^2}. \end{aligned} \quad (10)$$

In the transverse direction, transport is due to diffusion alone,

$$y^{n+1} = y^n + \sqrt{2D_T\Delta t}\eta_n \quad n = 0, 1, 2, \dots \quad (11)$$

For very large time steps, the solute has had time to sample the entire velocity field due to transverse diffusion. This is the timescale where the typical noise due to the transverse diffusive step reaches the distance over which the velocity field varies (l). This the Taylor timescale, or diffusive timescale, which we will call τ_D ,

$$\begin{aligned} l &= \sqrt{2D_T\tau_D} \\ \implies \tau_D &= \frac{l^2}{2D_T}. \end{aligned} \quad (12)$$

Fig. 1 (b) shows an example of where these timescales fall on the velocity autocorrelation function. It does indeed appear that the autocorrelation function begins to rise at around τ_r and has fallen again to near zero at around τ_D . If we assume that this is the case and that the autocorrelation function is symmetric in log space, then we can find the scaling of the peak location of the autocorrelation function in time, $\hat{\delta t}$,

$$\begin{aligned} \log \hat{\delta t} - \log \tau_r &= \log \tau_D - \log \hat{\delta t} \\ \implies \hat{\delta t}^2 &\sim \tau_r \tau_D \\ &\sim \frac{l^2 D_L}{\bar{u}^2 D_T}. \end{aligned} \quad (13)$$

$\hat{\delta t}$ is the geometric mean of τ_r and τ_D . This result also shows the need to differentiate between longitudinal and transverse diffusion. When the two are equal, this time is simply the characteristic advection time l/\bar{u} , but when they differ it changes. Now we can relate the peak in space ($\hat{\delta x}$) to the peak in time ($\hat{\delta t}$) as

$$\hat{\delta x} \sim \bar{u} \hat{\delta t} \sim l \sqrt{\frac{D_L}{D_T}}. \quad (14)$$

B. Validation

To ensure that the peak location scaling arguments presented in the prior subsection are valid, we tested them by running a series of numerical simulations. In each simulation, we track 10^5 particles whose initial condition is flux weighted along the line $x = 0$ and whose subsequent motion follows the Langevin equation (Eq. 4). We fix the baseline parameters

to $l = \bar{u} = 1$ and $D_L = D_T = 10^{-3}$ and then vary each of them over a range of values. We measure the autocorrelation functions in space and time as well as the locations of their peaks. The peaks in space and time are referred to as $\hat{\delta}x$ and $\hat{\delta}t$ respectively. Subscripts are used to show which velocity field was used: a subscript of c is used for Couette flow simulations and a subscript of p is used for Poiseuille flow simulations.

The results of this scaling analysis are shown in Fig. 3. The first parameter we consider is the distance over which the velocity field varies, l . As l increases, the distance a particle must travel to sample all of the velocities in the system increases, so the peak location will shift right, meaning the peak location will scale as some positive power of l , which, as we argue from Eqs. 13 and 14, should be 1. For Couette flow, $l = L$, the distance between the plates. For Poiseuille flow, the velocity field is symmetric, so it only varies over half of the domain length, $l = \frac{L}{2}$. Fig. 3 (a) shows that indeed, the location of the peak in the autocorrelation function scales linearly with l .

Next, we consider average velocity. For this case, the scaling of the peak location with regard to \bar{u} depends on whether the autocorrelation function is defined in space or in time. Eq. 13 suggests it scales inversely with average velocity in time, while Eq. 14 suggests that it is independent of mean velocity in space, which is again completely in line with our observations from simulations shown in Fig. 3 (b). If the average velocity is zero, then the system is diffusion dominated and the autocorrelation function will be near zero. On the other hand, as the average velocity increases, the system becomes more deterministic and highly correlated.

Finally, we consider diffusion. In the longitudinal direction, the existence of diffusion is the very reason the rise toward a peak in the autocorrelation function exists; thus as we increase diffusion in the longitudinal direction, D_L , we anticipate the location of the peak will also shift in the positive direction. From Eq. 13 we argue that the peak location should scale with the square root of D_L . Fig. 3 (c) shows that this is indeed the case. Transverse diffusion is the process that allows particles to sample the full variability of velocities in the system. Thus one can anticipate that an increase in the transverse diffusion coefficient will lead the location of the peak to shift toward smaller values. From Eq. 13 we anticipate a scaling which is proportional to $D_T^{-\frac{1}{2}}$, which is indeed what we observe in Fig. 3 (d). These scaling relations imply that the peak location depends on the *ratio* between longitudinal and transverse diffusion. In many applications, diffusion is considered to be isotropic, which, interestingly,

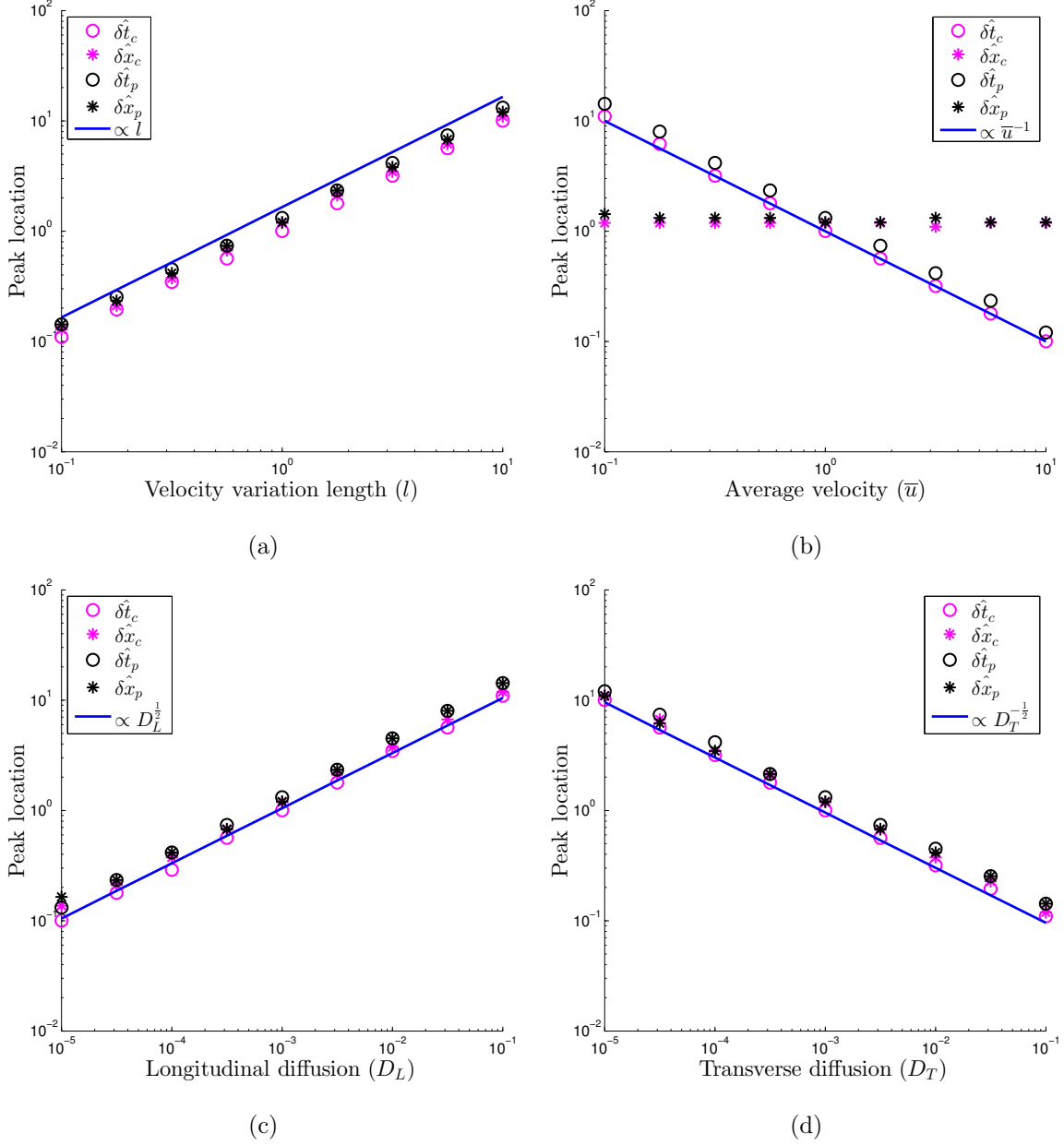


Figure 3: Location in time and space of the peak of the autocorrelation function ($R^*(\delta)|_{(1,2)}$) as a function of (a) the distance over which the velocity field varies (l), (b) the spatial average of the velocity field (\bar{u}), (c) longitudinal diffusion (D_L), and (d) transverse diffusion (D_T).

leads to the location of the peak in the autocorrelation function being *independent* of the diffusion coefficient, because these competing effects exactly balance one another.

While the actual scaling relationships that we had predicted all seem to hold in Fig. 3, one thing that does stand out is that specific values for Couette and Poiseuille flow are offset

from one another, suggesting that there is one more missing ingredient in this analysis. To identify this ingredient, we begin by decomposing the velocity field into its spatial average and fluctuations,

$$u(y) = \bar{u} + u'(y), \quad \bar{u} = \frac{1}{L} \int_0^L u(y) dy. \quad (15)$$

Then the spatial variance of the velocity field is

$$\overline{u'u'} = \frac{1}{L} \int_0^L u'(y)^2 dy. \quad (16)$$

From this we can say that for Couette and Poiseuille flow the velocity fields have variance

$$\overline{u'u'}_c = \frac{\bar{u}}{3} \quad \overline{u'u'}_p = \frac{\bar{u}}{5}, \quad (17)$$

respectively. Since the variance of velocity depends on which flow field we use, it may contribute to the missing ingredient in the scaling arguments which caused the peaks to offset. However, this only provides us with two points from which we cannot infer any reliable scaling behavior.

In order to determine the scaling of the peak location with regard to the variance in velocity, we ran an additional set of simulations. Thus far, we have only looked at two different velocity fields. Therefore, we only have two different values of the dimensionless coefficient of variation, $c_v = \frac{\sqrt{\overline{u'u'}}}{\bar{u}}$. In order to assess the scaling of the peak location with the coefficient of variation more velocity fields were needed. We defined a general stratified velocity field,

$$u_s(y) = \bar{u} + \sigma \gamma(y), \quad (18)$$

where $\sigma = \sqrt{\overline{u'u'}}$ is the parameter we varied and $\gamma(y)$ is a sorted sequence of random numbers with mean 0. This allowed us to create velocity fields with a large range of values for the variance and coefficient of variation. While such a velocity field may be deemed unphysical from the standpoint of a Navier-Stokes flow it could arise from a Darcy flow through a stratified aquifer [32–34], and the recent work of [35] also suggests that when chosen to represent the cumulative density function of longitudinal velocities in a highly complex heterogeneous flow, it can adequately represent and upscale transport.

The characteristic length scale in these systems is $l = L$, as in Couette flow. In all of these simulations, we set $L = \bar{u} = 1$ and $D_L = D_T = 10^{-3}$. Fig. 4 shows the locations of the

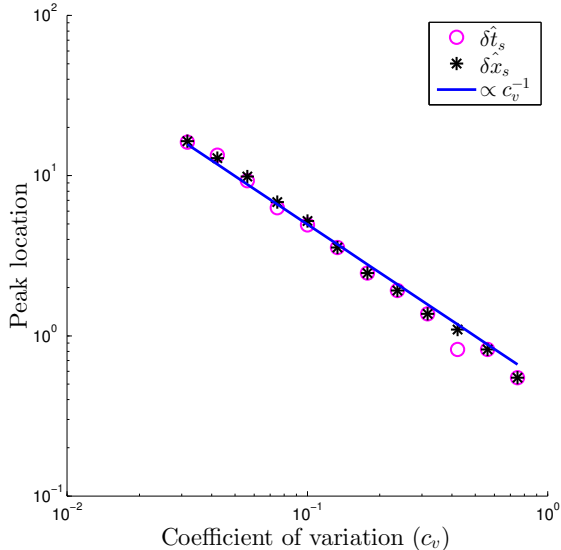


Figure 4: Location in time and space of the peak of the autocorrelation function $(R^*(\delta))|_{(1,2)}$ versus the coefficient of variation (c_v) for stratified velocity fields defined in Eq. 18.

peaks of the autocorrelation functions obtained from this set of simulations. We find that the locations of the peaks in the autocorrelation are approximately proportional to c_v^{-1} . At first, this scaling may seem counterintuitive. The reason for this is that if the velocity field has no variance at all, then the system is purely diffusive, thus no correlation exists, so the autocorrelation function can never take the assumed form (i.e., it will never increase to a peak).

This evidence indicates that the non-dimensional peak locations, $\frac{\hat{\delta}x}{l}$ and $\frac{\hat{\delta}t\bar{u}}{l}$ are proportional to the dimensionless quantity $c_v^{-1} \sqrt{\frac{D_L}{D_T}}$. Thus, we can collapse all of the peak locations in time to a single line and likewise for the peaks in space. These lines are shown in Fig. 5. The peak locations are represented well by these lines. The proportionality constants for this linear scaling are found to be equal for both as $\alpha = 0.6$.

IV. SPATIAL MARKOV MODEL

As noted in the introduction, the purpose of this note is to find the limits of the Spatial Markov model, which has been used to successfully replicate transport behavior in heterogeneous velocity fields, such as those of interest here. Here we provide a description of this

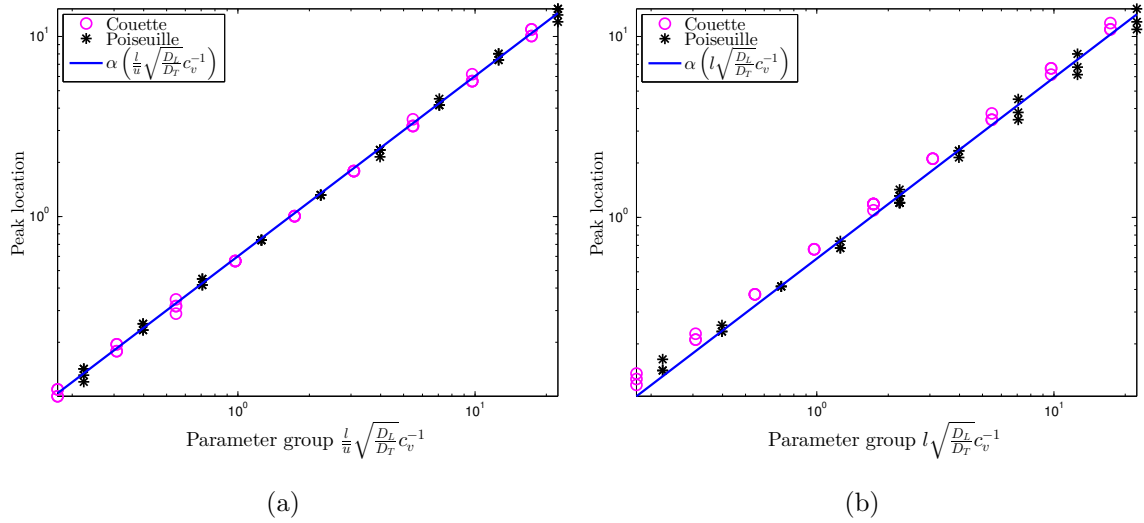


Figure 5: Peak location in (a) time versus the parameter group $\frac{l}{\bar{u}} \sqrt{\frac{D_L}{D_T}} c_v^{-1}$ and in (b) space versus the parameter group $l \sqrt{\frac{D_L}{D_T}} c_v^{-1}$.

upscaled model. The Spatial Markov model falls into the broader category of continuous time random walk models (CTRW). In a CTRW model, the solute mass is discretized into a large number of particles whose motion is governed by the Langevin equations,

$$\begin{aligned}
 x_{n+1} &= x_n + \delta x \\
 t_{n+1} &= t_n + \tau_n \quad n = 0, 1, 2, \dots
 \end{aligned}
 \tag{19}$$

where in this representation δx is a fixed spatial increment and $\{\tau_n\}$ are random motion times described by some chosen distribution $f(\tau_1, \tau_2, \dots)$. This matches the upscaled interpretation depicted on the right hand side of Fig. (2). This is similar to Eq. 4 except that now only longitudinal transport is modeled and we do not require that time steps are fixed, but rather that they can be random. In general CTRW models δx may also be random [11], but in our Spatial Markov implementation it is fixed.

What really distinguishes the Spatial Markov model from other similar models is that it does not use independent and identically distributed $\{\tau_n\}$ values from a given univariate distribution, but rather models a one-step correlation between successive values using a Markov Chain. This means that $\{\tau_n\}$ values are described by the conditional distribution

$$f(\tau_n) = \begin{cases} f(\tau_1) & \text{for } n = 1 \\ f(\tau_n|\tau_{n-1}) & \text{for } n = 2, \dots \end{cases} \quad (20)$$

Numerically, we approximate $f(\tau_n|\tau_{n-1})$ by discretizing the marginal $f(\tau_1)$ into β travel time classes, or bins. If $\beta = 1$, the model reduces to an uncorrelated model. As β increases, more of the correlation structure of the system is resolved. We model the steps of the Spatial Markov model as a spatially homogeneous Markov process with β discrete states, which can be described with a transition probability matrix, T_{ji} , defined as,

$$T_{ji} = P(\tau_{n+1} \in \text{bin } j | \tau_n \in \text{bin } i) = P(\tau_2 \in \text{bin } j | \tau_1 \in \text{bin } i). \quad (21)$$

Practically speaking, in order to do this, we simulate transport using the Langevin equation (Eq. 4) over a distance of $x = 2\delta x$ and measure the time it takes for each particle to cross $x = \delta x$ and $x = 2\delta x$. This gives us the joint distribution of particle travel times $f(\tau_1, \tau_2)$. We then choose the classes, as is commonly done, by splitting $f(\tau_1)$ into β equiprobable regions and recording the values of τ_1 corresponding to the boundaries of these regions. The smallest travel times belong to bin 1, and a particle's travel time is in bin i if $t_i \leq \tau < t_{i+1}$, where t_i is the lower limit of bin i , which for bin 1 is 0. In steady flows, T_{ji} tends to be a diagonally dominant banded matrix, indicating that particles have the highest probability of staying in their initial class, with some probability of jumping to nearby classes. Further details of the procedure for creating a Spatial Markov model are available in [13, 15, 18].

The strength of the Spatial Markov model is that by not imposing that τ_{n+1} be independent of τ_n , we reduce the minimum length scale over which the $\{\tau_n\}$ may be measured and still create a valid model. We need not wait until asymptotic time to begin measuring the travel time distribution. But to determine how much this length scale is reduced, we must consider the assumptions of the model and when they are valid.

A. Model Assumptions

There are two key assumptions that must be met for the Spatial Markov model to be a valid approach. First, the Spatial Markov model assumes that between any two adjacent spatial jumps, the correlation structure is the same (i.e., spatially homogeneous). Furthermore, treating transport as a Markov Chain requires that a particle's next state only depends

on its current state regardless of how the particle arrived in its current state or how long it has been there. This means that the number of steps (each corresponding to a length δx) required to leave the current state follows a geometric distribution and the autocorrelation between subsequent steps is exponential [21, 30, 36]. Since each state has a distinct range of velocities assigned to it, this exponential autocorrelation passes into the velocity domain. In order to satisfy these assumptions we require the autocorrelation function between velocities averaged over a distance δx^* and separated by a distance $|j - i|\delta x^*$ for $|j - i| \in \mathbb{N}$ be exponential. That is,

$$\hat{R}^x(i, j)|_{\delta x^*} = \underbrace{\hat{R}^x(|j - i|)|_{\delta x^*}}_{\text{spatially homogeneous}} = \underbrace{\exp(a_{\delta x^*}|j - i|)}_{\text{Markov process}}, \quad (22)$$

where $a_{\delta x^*} \in \mathbb{R}^-$ depends on δx^* and can be related to the second largest eigenvalue of the transition matrix (T_{ji}) [37]. The function $\hat{R}^x(i, j)|_{\delta x^*}$ is distinct from $R^x(i, j)|_{\delta x}$ in that it is the autocorrelation function required to satisfy the assumptions of the Spatial Markov model, as opposed to the actual measured autocorrelation function.

B. Implications of the Model Assumptions

The next step is to find what the restriction on $R^x(i, j)|_{\delta x}$ means for $R^x(\delta x)|_{(1,2)}$. From this information, we can determine the length scale over which the assumptions of the Spatial Markov model hold (δx^*) by finding the scale where $R^x(\delta x)|_{(1,2)}$ behaves in the required way. In order to derive the requirements on $R^x(\delta)|_{(1,2)}$, we assume $R^t(i, j)|_{\delta t} = \hat{R}^t(i, j)|_{\delta t^*}$ and propagate the correlation to larger δt . The analysis is shown in Appendix A. We find that $R^t(\delta)|_{(1,2)}$ must have a negative first derivative and positive second derivative and we assume that $R^x(\delta)|_{(1,2)}$ must satisfy the same restriction. This seems reasonable, since if we were to analyze the autocorrelation between travel times directly (rather than using the average velocities in space), then the analysis would be nearly identical to that in Appendix A.

As we have seen above (Fig.1), the actual autocorrelation function $R^x(\delta)|_{(1,2)}$ does not satisfy these properties at all scales. Thus, in order to satisfy the assumptions of the Spatial Markov model, we must ensure that the length scale over which the model is applied (δx) is sufficiently large that at distances greater than δx , $R^x(\delta x)|_{(1,2)}$ has a negative first derivative and positive second derivative. Since $R^x(\delta x)|_{(1,2)}$ is clearly concave down at its peak, we seek

the length scale where $R^{x''}(\delta x)|_{(1,2)} > 0$ as the length scale over which velocity distributions are taken. Thus we are seeking the inflection point (after the peak) in the autocorrelation function. Note that, while the primary focus of this work is on the Spatial Markov model, many of the arguments presented would also hold for a Temporal Markov model [e.g. 38]. Choosing between the two depends on the specific system of interest [13].

V. PEAK AND INFLECTION POINT RELATIONSHIP

The inflection points are found by locating the zero in the second derivative of $R^x(\delta x)|_{(1,2)}$ for all of the simulations. We compute the second derivative numerically using an eighth order accurate finite difference method to eliminate measurement noise; however, the inferred inflection point locations are still quite noisy. An alternative method to find the inflection points, which would eliminate some of the noise, would be to assume the form of the autocorrelation function and fit an analytical curve through it. However, due to the additional assumption required for this method, we opt to find the inflection points numerically.

The locations of inflection points and the peaks have a linear relationship, shown in Fig. 6. The variance in the inflection point locations, however, depends on the location of the peak. This can be seen in the figure by noting that the scatter in the data is fairly uniform on a log scale. This means that a standard least squares linear fit is insufficient to estimate the standard error. We therefore fit the log of the inflection point locations to the log of the peak locations. The fit of $\delta x^* = 2.3\hat{\delta x}$ is shown in blue with the standard error (± 1.3) shaded in red. This means that the non-dimensional inflection point locations, $\frac{\delta x^*}{l}$ and $\frac{\delta t^* \bar{u}}{l}$ are approximately equal to $(2.3 \pm 1.3)(.6)c_v^{-1} \sqrt{\frac{D_L}{D_T}}$. Thus, to be conservative, we will use $\delta x^* = 2.2 \frac{l}{c_v} \sqrt{\frac{D_L}{D_T}}$, which accounts for the standard error.

VI. SPATIAL MARKOV MODEL PERFORMANCE AT, AND ON EITHER SIDE OF, δx^*

Now that we have an estimate for the location of the inflection points in space (δx^*) of the autocorrelation functions, we can test the effect of using the Spatial Markov model with δx in Eq. 19 set to various multiples of δx^* . If these inflection point locations are indeed the cutoff between where the Spatial Markov model is valid and not, then when we use $\delta x < \delta x^*$,

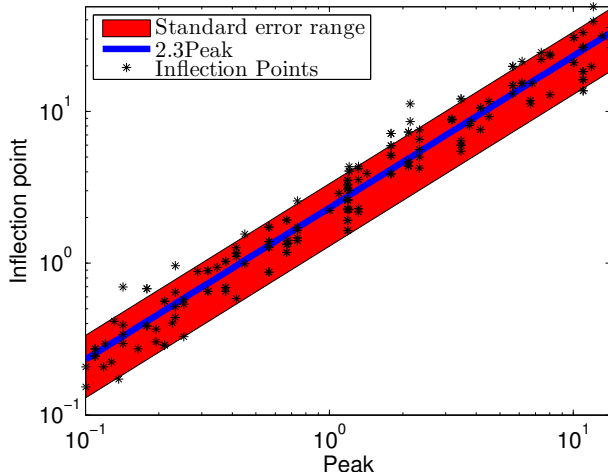


Figure 6: Inflection point locations versus peak locations.

the model should fail to predict transport metrics properly, but when we use $\delta x \geq \delta x^*$, the model should yield reasonable predictions.

To test this, we set $L = \bar{u} = 1$ and $D_L = D_T = 10^{-3}$ and simulate the transport of 10^6 particles using Eq. 4. We parameterize the Spatial Markov model and then compare predictions to results from fully resolved microscale simulations that solve Eq. 4 up to large timescales. The results of these microscale simulations are referred to as benchmarks, because all of the physics are highly resolved within them so they can be used to determine the accuracy of the Spatial Markov models.

The first metric we use for comparison is the second centered moment of the plume (Eq. 6). Fig. 7 shows the predictions of the Spatial Markov models using ten bins ($\beta = 10$) with different values of δx along with the benchmarks for both velocity fields. The models using $\delta x < \delta x^*$ predict values of $\sigma^2(t)$ that are below the benchmarks, implying these models are unable to capture all of the spreading that takes place. The models using $\delta x \geq \delta x^*$ perform much better, implying that they are able to capture more of the true physical behavior of the systems. While a difference can be seen between the two models using $\delta x < \delta x^*$, the predictions of the three models with $\delta x \geq \delta x^*$ are indistinguishable from each other. This implies that as long as δx is at least as large as the critical length scale (δx^*), then doubling and even quadrupling does not add to the performance of the Spatial Markov model.

The other metric used for comparison is the autocorrelation function $R^x(i, j)|_1$. This comes with an added benefit and allows us to get some insight into an open question which

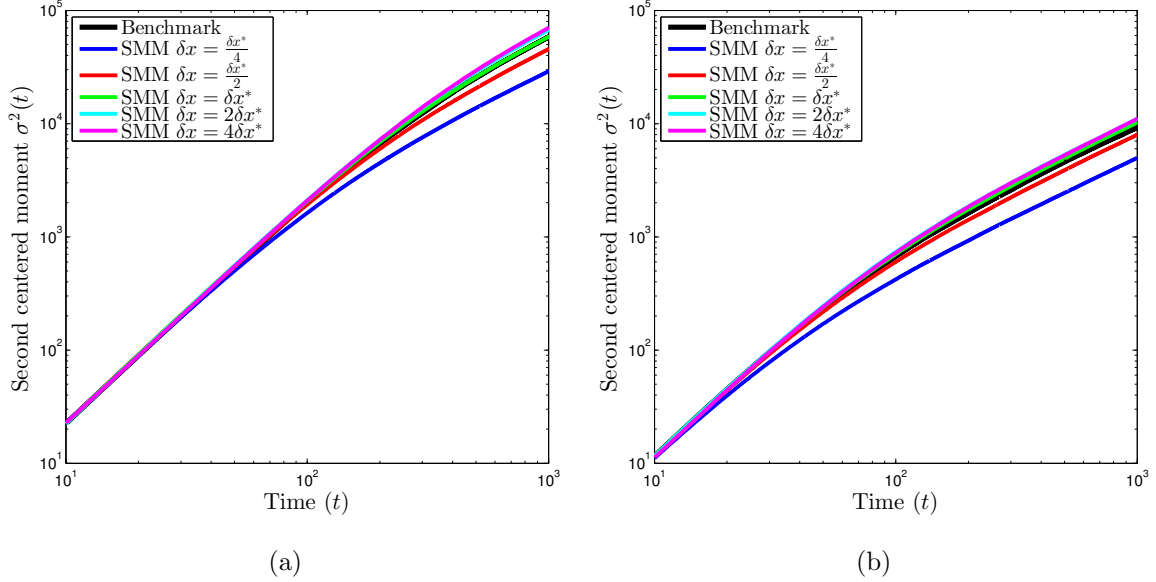


Figure 7: Spatial Markov model predictions of the second centered spatial moment of the plume ($\sigma^2(t)$) using breakthrough data at and on either side of δx^* for (a) Couette flow and (b) Poiseuille flow.

remains: how many discrete travel time classes (β) must be used in order to create a reliable Spatial Markov model? In order to answer this question, we compare the predictions of the assumed form of the autocorrelation function $\hat{R}^x(i, j)|_1$ (Eq. 22) of many Spatial Markov models with varying δx and varying number of velocity classes (β). The only free parameter in this equation is the spatial decorrelation rate, a_1 , so we fit an exponential curve through the function $R^x(i, j)|_1$ for each of the Spatial Markov models and compare their predicted value of a_1 to the benchmark value which is found by fitting an exponential through $R^x(i, j)|_1$ from the fine scale simulation.

Fig. 8 illustrates the effect of changing the length scale over which the model is used (δx) and the effect of changing the number of bins (β) on the predicted value of a_1 . We see that while for small values of β the prediction of a_1 improves as δx gets larger, as long as $\beta \geq 10$, increasing δx beyond δx^* leads to very little improvement. Thus, if the Spatial Markov model is to be used with the smallest valid length scale ($\delta x = \delta x^*$), then the travel time distribution $f(\tau_1)$ should be discretized into at least 10 different classes, creating a transition matrix that is at least 10x10. It is important to note that this finding is not physically based, but made only from empirical observation; however it does agree very well with similar empirical observations of [15]. Note that this discretization of the transition

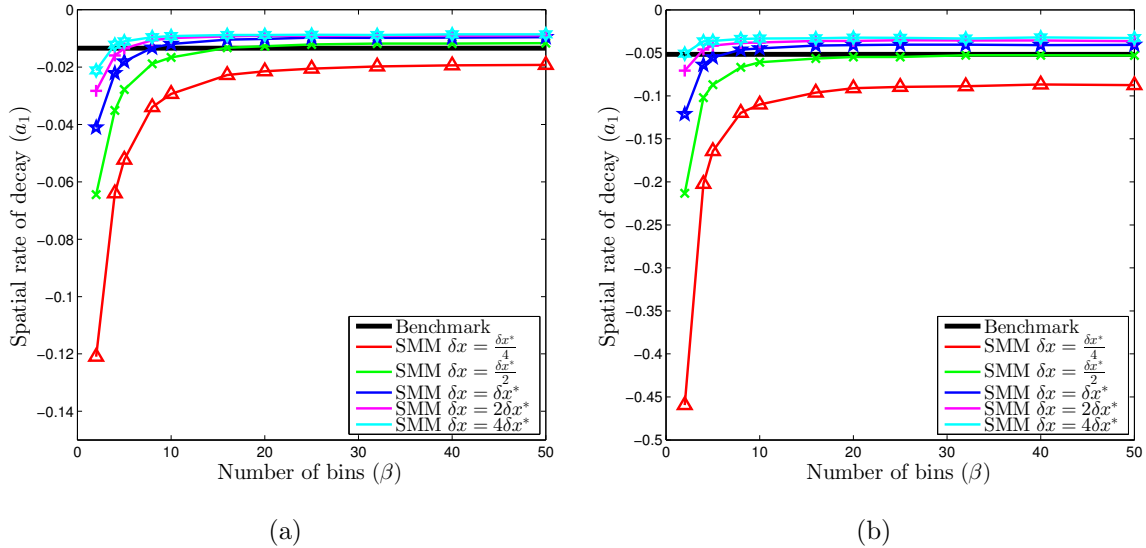


Figure 8: Spatial Markov model predictions of a_1 , the spatial rate of decay of the autocorrelation function, versus β , the number of travel time bins, modeled using different values of δx for (a) Couette flow and (b) Poiseuille flow.

matrix issue is associated with the manner in which we, and most studies to date, generate the transition matrix. If one had a way to generate the transition probability density in a non-discrete continuous way, no such issue would arise.

VII. CONCLUSION

In this paper we have aimed to address an open question: What is the smallest scale at which the Spatial Markov model can be used for upscaling transport in a heterogeneous velocity field? To address this issue we focus on a classical and well studied class of velocity fields: pure shear flows. The theory developed here can be used to guide the choice of this modeling length scale, which we denote as δx^* . While the theory developed in this note was validated only in these very simple velocity fields, the scaling arguments did not require any particular form of the velocity fields, so the ideas should be readily extendable to a broad range of flow fields, although additional considerations must be made for velocity fields that change in the longitudinal direction. Such considerations include flow heterogeneity at multiple scales, and large contrasts between highly mobile and stagnant regions of varying size, all of which may influence the scaling arguments presented here and are worthy of

future study. For example, a fundamental assumption of the Spatial Markov model is that the velocity field statistics are stationary over the length scale used in the model. While this was of no concern in the velocity fields used here, it must be accounted for in general. If, by use of the theory presented in this note, one were to find δx^* to be smaller than the length scale over which the velocity field statistics are stationary, then the larger length scale must be used for the Spatial Markov model.

Concerning δx^* , from the work presented in this note, we conclude:

1. There exists an early time (and space) regime in which diffusion dominates advection in the longitudinal direction, which causes the autocorrelation between consecutive average velocities in time and space to be non-monotonic; first it rises and then it falls. This non-monotonic behavior suggests the existence of a length scale below which the Spatial Markov model is invalid.
2. In order to satisfy the assumptions of the Spatial Markov model, the autocorrelation function must be monotonically decreasing and concave up (first derivative always negative and second derivative always positive). The results of our analysis suggest that this minimum spatial scale $\delta x^* \sim \frac{l}{c_v} \sqrt{\frac{D_L}{D_T}}$, where l is length scale over which the velocity varies, c_v is the coefficient of variation of the velocity field and D_L and D_T are longitudinal and transverse dispersion coefficients respectively.

The Spatial Markov model has in several instances been shown to work very well at pre-asymptotic scales in advection dominated system, and this work helps to show why this is the case. Recall that the time scale after which asymptotic models are valid is the Taylor timescale, $\tau_D \sim \frac{L^2}{D_T}$, with the equivalent spatial scale equivalent being $\chi_D \sim \bar{u} \frac{l^2}{D_T}$. Here we have shown that the Spatial Markov model is valid after the spatial scale $\chi_{SMM} \sim \frac{l}{c_v} \sqrt{\frac{D_L}{D_T}}$. This means $\frac{\chi_{SMM}}{\chi_D} = \frac{\sqrt{D_L D_T}}{\bar{u} l c_v}$, which is like an inverse Peclet number, meaning that the Spatial Markov scale can be significantly smaller than the Taylor scale in advection dominated systems.

Acknowledgements This material is based upon work supported by, or in part by, NSF grants EAR-1351625, EAR-1417264 and EAR-1446236. Any opinions, findings, conclusions, or recommendations do not necessarily reflect the views of the funding agencies.

Appendix A: Appendix: Correlation propagation

In order to determine the implications of the restriction that $R^*(i, j)|_\delta$ be exponential on $R^*(\delta)|_{(1,2)}$, we consider the case where $\delta = \delta t$ as opposed to δx . This substantially simplifies the analysis. We simplify further by considering the case where average velocities over δt^* , $(v_i^t(\delta t^*))$ all have the same mean and variance.

To begin, recall, $v_i^t(\delta t) = \frac{\lambda_i}{\delta t}$ from Eq. 7. Then

$$v_i^t(n\delta t) = \frac{\sum_{j=(i-1)n+1}^{in} \lambda_j}{n\delta t}. \quad (\text{A1})$$

Now let $\rho_k = \hat{R}^t(|j - i| = k)|_{\delta t^*} = \exp(a_{\delta t^*} k)$ for $a_{\delta t^*} \in \mathbb{R}^-$, $k \in \mathbb{N}$. Since $\hat{R}^t(k)|_{\delta t^*}$ is exponential, $\rho_k = \rho_1^k$. Because the covariance operator is linear, we only need the pairwise covariance to find what $\hat{R}^t(n\delta t^*)|_{(1,2)}$, the autocorrelation between sequential average velocities over the interval $n\delta t^*$ given the form of $\hat{R}^t(k)|_{\delta t^*}$, must be. The pairwise covariance is,

$$\text{Cov}[v_i, v_j] = \begin{cases} \sigma_{\delta t^*}^2 & i = j \\ \rho_{|j-i|} \sigma_{\delta t^*}^2 & i \neq j, \end{cases} \quad (\text{A2})$$

where $\sigma_{\delta t^*}^2$ is the variance of velocities averaged over δt^* , which for the sake of this analysis is taken to be constant.

Then

$$\begin{aligned} \hat{R}^t(n\delta t^*)|_{(1,2)} &= \frac{\text{Cov} \left[\sum_{i=1}^n \frac{\lambda_i}{n\delta t^*}, \sum_{j=n+1}^{2n} \frac{\lambda_j}{n\delta t^*} \right]}{\sqrt{\text{Cov} \left[\sum_{i=1}^n \frac{\lambda_i}{n\delta t^*}, \sum_{j=1}^n \frac{\lambda_i}{n\delta t^*} \right] \text{Cov} \left[\sum_{i=n+1}^{2n} \frac{\lambda_j}{n\delta t^*}, \sum_{j=n+1}^{2n} \frac{\lambda_j}{n\delta t^*} \right]}} \\ &= \frac{\frac{\sigma_{\delta t^*}^2}{(n\delta t^*)^2} \sum_{i=1}^n \sum_{j=n+1}^{2n} \rho_{j-i}}{\frac{\sigma_{\delta t^*}^2}{(n\delta t^*)^2} \left(n + 2 \sum_{j=1}^n \sum_{i=1}^{j-1} \rho_{j-i} \right)}. \end{aligned} \quad (\text{A3})$$

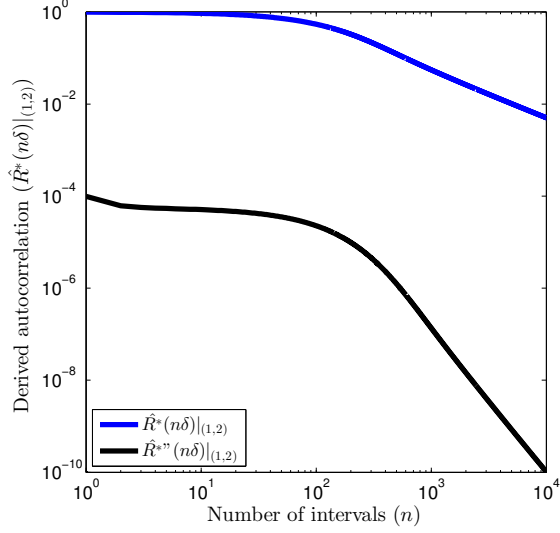


Figure 9: Derived autocorrelation function $\hat{R}^*(n\delta)|_{(1,2)}$, which satisfies the assumptions of the Spatial Markov model, and its second derivative with $a_\delta = -10^{-2}$.

Recognizing that both the numerator and denominator are geometric series, we find that

$$\begin{aligned} \hat{R}^t(n\delta t^*)|_{(1,2)} &= \frac{\rho_1 \left(\frac{1-\rho_1^n}{1-\rho_1}\right)^2}{n + 2\rho_1 \frac{-(1-\rho_1^n) + n(1-\rho_1)}{(1-\rho_1)^2}} \\ &= \frac{\rho_1 (1 - \rho_1^n)^2}{n(1 - \rho_1^2) + 2\rho_1(\rho_1^n + 1)}. \end{aligned} \quad (\text{A4})$$

Fig. 9 shows this function for $a_\delta = -10^{-2}$. Regardless of the particular value of a , as long as it is in \mathbb{R}^- , $\hat{R}^t(n\delta t^*)|_{(1,2)}$ is monotonically decreasing and its second derivative is always positive.

-
- [1] G. Taylor, Dispersion of soluble matter in solvent flowing slowly through a tube, *Proc. R. Soc. Lond. Math. Phys. Sci.* 219 (1137) (1953) 186–203.
- [2] R. Aris, On the dispersion of a solute in a fluid flowing through a tube, *Proc. R. Soc. Lond. Math. Phys. Sci.* 235 (1200) (1956) 67–77.
- [3] H. Brenner, Dispersion resulting from flow through spatially periodic porous media, *Philos. Trans. R. Soc. Lond. Math. Phys. Sci.* 297 (1430) (1980) 81–133.
- [4] S. Whitaker, *The Method of Volume Averaging*, Vol. 13, Springer, 1998.
- [5] U. Hornung, *Homogenization and Porous Media*, *Interdisciplinary Applied Mathematics*, Vol. 6, Springer-Verlag, New York, 1997.
- [6] M. Dentz, H. Kinzelbach, S. Attinger, W. Kinzelbach, Temporal behavior of a solute cloud in a heterogeneous porous medium: 1. point-like injection, *Water Resour. Res.* 36 (12) (2000) 3591–3604.
- [7] T. Le Borgne, M. Dentz, J. Carrera, Spatial Markov processes for modeling lagrangian particle dynamics in heterogeneous porous media, *Physical Review E* 78 (2008) 026308.
- [8] D. A. Benson, S. W. Wheatcraft, M. M. Meerschaert, The fractional-order governing equation of Lévy motion, *Water Resour. Res.* 36 (6) (2000) 1413–1423.
- [9] J. H. Cushman, T. R. Ginn, Fractional advection-dispersion equation: a classical mass balance with convolution-Fickian flux, *Water Resour. Res.* 36 (12) (2000) 3763–3766.
- [10] E. W. Montroll, G. H. Weiss, Random walks on lattices. ii, *J. Math. Phys.* 6 (2) (1965) 167–181.
- [11] B. Berkowitz, A. Cortis, M. Dentz, H. Scher, Modeling non-Fickian transport in geological formations as a continuous time random walk, *Rev. Geophys.* 44 (2).
- [12] R. Haggerty, S. M. Gorelick, Multiple-rate mass transfer for modeling diffusion and surface reactions in media with pore-scale heterogeneity, *Water Resour. Res.* 31 (10) (1995) 2383–2400.
- [13] T. Le Borgne, M. Dentz, J. Carrera, Lagrangian statistical model for transport in highly heterogeneous velocity fields, *Physical Review Letters* 101 (2008) 090601.
- [14] P. Kang, M. Dentz, T. L. Borgne, R. Juanes, Spatial markov model of anomalous transport through random lattice networks, *Physical Review Letters* 107 (2011) 180602.
- [15] T. Le Borgne, D. Bolster, M. Dentz, P. Anna, A. Tartakovsky, Effective pore-scale disper-

- sion upscaling with a correlated continuous time random walk approach, *Water Resour. Res.* 47 (12) (2011) W12538.
- [16] P. de Anna, T. Le Borgne, M. Dentz, A. M. Tartakovsky, D. Bolster, P. Davy, Flow intermittency, dispersion, and correlated continuous time random walks in porous media, *Phys. Rev. Lett.* 110 (2013) 184502.
- [17] P. K. Kang, P. Anna, J. P. Nunes, B. Bijeljic, M. J. Blunt, R. Juanes, Pore-scale intermittent velocity structure underpinning anomalous transport through 3-d porous media, *Geophysical Research Letters* 41 (17) (2014) 6184–6190.
- [18] D. Bolster, Y. Méheust, T. L. Borgne, J. Bouquain, P. Davy, Modeling preasymptotic transport in flows with significant inertial and trapping effects - the importance of velocity correlations and a spatial Markov model, *Adv. Water Resour.* 70 (0) (2014) 89 – 103.
- [19] N. Sund, D. Bolster, S. Mattis, C. Dawson, Pre-asymptotic transport upscaling in inertial and unsteady flows through porous media, *Transport in Porous Media* 109 (2) (2015) 411–432.
- [20] N. L. Sund, D. Bolster, C. Dawson, Upscaling transport of a reacting solute through a periodically converging–diverging channel at pre-asymptotic times, *Journal of contaminant hydrology* 182 (2015) 1–15.
- [21] P. K. Kang, T. Le Borgne, M. Dentz, O. Bour, R. Juanes, Impact of velocity correlation and distribution on transport in fractured media: Field evidence and theoretical model, *Water Resources Research* 51 (2) (2015) 940–959.
- [22] P. Wang, G. Chen, *International Journal of Heat and Mass Transfer* 95 (2016) 131–141.
- [23] M. Dejam, H. Hassanzadeh, Z. Chen, Shear dispersion in a capillary tube with a porous wall, *Journal of Contaminant Hydrology*.
- [24] F. Hains, Stability of plane couette-poiseuille flow, *Physics of Fluids (1958-1988)* 10 (9) (1967) 2079–2080.
- [25] J. Bear, L. G. Fel, Y. Zimmels, Effects of material symmetry on the coefficients of transport in anisotropic porous media, *Transport in porous media* 82 (2) (2010) 347–361.
- [26] H. Risken, *Fokker-Planck Equation*, Springer, 1984.
- [27] W. Young, Arrested shear dispersion and other models of anomalous diffusion, *Journal of Fluid Mechanics* 193 (1988) 129–149.
- [28] U. M. Scheven, P. N. Sen, Spatial and temporal coarse graining for dispersion in randomly packed spheres, *Physical review letters* 89 (25) (2002) 254501.

- [29] M. Dentz, J. Carrera, Mixing and spreading in stratified flow, *Physics of Fluids* (1994-present) 19 (1) (2007) 017107.
- [30] P. K. Kang, M. Dentz, T. Le Borgne, R. Juanes, Anomalous transport on regular fracture networks: Impact of conductivity heterogeneity and mixing at fracture intersections, *Physical Review E* 92 (2) (2015) 022148.
- [31] G. Delic, M. F. Wheeler, *Next Generation Environmental Models and Computational Methods*, Vol. 87, Siam, 1997.
- [32] G. Matheron, G. de Marsily, Is transport in porous media always diffusive? a counterexample, *Water Resources Research* 16 (1980) 901.
- [33] V. Zavala-Sanchez, M. Dentz, X. Sanchez-Vila, Characterization of mixing and spreading in a bounded stratified medium, *Advances in water resources* 32 (5) (2009) 635–648.
- [34] D. Bolster, F. J. Valdes-Parada, T. LeBorgne, M. Dentz, J. Carrera, Mixing in confined stratified aquifers, *Journal of Contaminant Hydrology* 120 (2011) 198–212.
- [35] G. Porta, B. Bijeljic, M. Blunt, A. Guadagnini, Continuum-scale characterization of solute transport based on pore-scale velocity distributions, *Geophysical Research Letters* 42 (18) (2015) 7537–7545.
- [36] L.-P. Wang, D. E. Stock, Stochastic trajectory models for turbulent diffusion: Monte carlo process versus markov chains, *Atmospheric Environment. Part A. General Topics* 26 (9) (1992) 1599–1607.
- [37] W. S. Kendall, F. Liang, *Markov chain Monte Carlo: innovations and applications*, Vol. 7, World Scientific, 2005.
- [38] D. Meyer, H. Tchelepi, Particle-based transport model with markovian velocity processes for tracer dispersion in highly heterogeneous porous media, *Water Resources Research* 46 (2010) W11552.